WAVE-EQUATION INTERFEROMETRIC MIGRATION OF VSP DATA

by

Ruiqing He

A dissertation submitted to the faculty of
The University of Utah
in partial fulfillment of the requirements for the degree of

Doctor of Philosophy
in
Geophysics

Department of Geology and Geophysics

The University of Utah

May 2006

THE UNIVERSITY OF UTAH GRADUATE SCHOOL

SUPERVISORY COMMITTEE APPROVAL

of a dissertation submitted by

Ruiqing He

This dissertation has been read by each member of the following supervisory committee and by majority vote has been found to be satisfactory.

	Chair: Gerard T. Schuster
	Robert B. Smith
	Cari Johnson
	Christopher Sikorski
	Yue Wang

THE UNIVERSITY OF UTAH GRADUATE SCHOOL

FINAL READING APPROVAL

To the Graduate Council of the University of Utah:

I have read the dissertation of Ruiqing He in its final form and have found that (1) its format, citations, and bibliographic style are consistent and acceptable; (2) its illustrative materials including figures, tables, and charts are in place; and (3) the final manuscript is satisfactory to the Supervisory Committee and is ready for submission to The Graduate School.

Date

Gerard T. Schuster
Chair, Supervisory Committee

Approved for the Major Department

Marjorie A. Chan
Chair/Dean

Approved for the Graduate Council

David S. Chapman
Dean of The Graduate School

ABSTRACT

Interferometric migration (IM) is a recently developed method that is proved to be a powerful imaging tool for VSP data. Synthetic and field data examples demonstrate that IM is robust to velocity estimation errors, and can sometimes produce reflectivity images much more accurate than standard migration methods. In this thesis, a wave-equation interferometric migration (WEIM) method is developed for 3D migration of VSP multiples. With WEIM, for each receiver gather of 3D VSP data, only one 3D receiver gather of travel times and one 3D wavefield extrapolation need to be calculated for the migration of free-surface multiples. Compared to the expensive acquisition and processing costs of a 3D surface seismic survey, the tremendous efficiency in obtaining a 3D subsurface image volume by migration of 3D VSP free-surface multiples suggests that a 3D VSP survey might also serve as a cost effective 4D monitoring tool for some oil fields. WEIM is also applied to image vertical subsurface structures, such as salt flanks which are difficult to image by conventional surface seismic surveys.

To my family.

CONTENTS

LIST OF FIGURES

ACKNOWLEDGMENTS

First, I would like to thank my supervisor, Dr. Gerard Schuster, for his enlightening lectures, innovative discussions, guidance and support throughout my years at the University of Utah.

Second, I am in debt to other members of my advisory committee: Dr. Robert Smith, Dr. Cari Johnson, Dr. Christopher Sikorski, and Dr. Yue Wang. They have broadened my horizons in the fields of seismology, stratigraphy, scientific computation and seismic exploration. I also would like to thank the UTAM sponsors during these years for financial support. Staffs at CHPC also have been helpful for providing computational facilities.

At last, I would like to dedicate this dissertation to my family for their sacrifice and unconditional support.

CHAPTER 1

INTRODUCTION AND OVERVIEW

Interferometric migration (IM) is a new seismic imaging tool that analyzes interference patterns in recorded seismic data. Analogous to optical interferometry, seismic interferometry estimates the detailed properties of an elastic medium by analyzing the interference patterns of seismic waves. The interference patterns are constructed by correlating seismic traces with one another and can sometimes be used to more robustly image the earth's elastic properties compared to standard seismic imaging.

In this chapter, the research background, basic principles and properties of seismic interferometry are first introduced. This is followed by an overview of my work in this thesis. My primary original contribution is the development of a 3D wave-equation interferometric migration (WEIM) method for efficient processing of 3D VSP data. The WEIM method is also used to image vertical subsurface structures, such as salt flanks which are usually difficult to image by surface seismic methods.

1.1 Interferometric Migration (IM)

1.1.1 Research Background

The key idea underlying seismic interferometry dates back to Claerbout's passive seismic imaging concept. Claerbout (1968) showed that, for a 1-D velocity model, the positive time portion of the autocorrelation of a seismogram due to an impulsive source at depth is the seismogram due to an impulsive source on the surface. This implies that earthquake-induced seismograms can be transformed into shot gathers used by exploration seismologists. One outstanding advantage of this passive seismic imaging method is that the features of the earthquake source, such as location and initial excitation time, are not needed. In order to verify this, Cole (1995) conducted a field experiment with seismic data recorded by a 4000 channel 2-D array of geophones on the Stanford University campus. Unfortunately, possibly due to the short (20 minute) records or bad

coupling between the geophones and the dry California soil, his results were inconclusive. Later, Daneshvar et al. (1995) successfully imaged the subsurface reflectivity distribution by autocorrelating seismograms recorded on the island of Hawaii that were generated from vertically incident microearthquakes. These pseudo-reflection seismograms showed reasonable agreement with a refraction study in the area.

Later, Rickett and Claerbout (1996) generated synthetic data with the phase-shift method (Gazdag, 1978; Gazdag and Sguazzero, 1984) by crosscorrelating traces with one another. These correlated traces showed the same kinematics for reflection arrivals generated by surface shots for both point diffractors and planar reflector models. Rickett and Claerbout (1999) then experimented with moving the passive source location close to the receivers and reflectors, and included modeling with a $v(x,z)$ velocity model. They observed that these changes did indeed affect the kinematics of the correlograms, but changes were small, and would probably not cause the method to fail in practical situations. Daylight imaging was conjectured to be a useful passive imaging tool if there was a random source distribution below the reflectors.

The same concept was rediscovered independently by the helioseismologists (Duvall et al., 1993), who created *time − distance* curves by cross-correlating passive solar dopplergrams recorded by the Michelson Doppler Imager (Scherrer et al., 1995). Point-to-point traveltimes derived from these time-distance curves could then be used in a range of helioseismic applications (e.g. Giles et al., 1997). If helioseismic time-distance curves are averaged spatially, the result is equivalent to a multi-dimensional autocorrelation. Rickett and Claerbout (2000) demonstrated that multi-dimensional spectral factorization provides spatially averaged time-distance curves with more resolution than those calculated by autocorrelation. However, their demonstration was restricted to layered models with no lateral velocity variation.

Applying passive seismic imaging to VSP data, Katz (1990) received a patent in which he showed that 1-D images of the earth's reflectivity could be obtained by autocorrelating the traces recorded on the free-surface due to a rotating drill bit. Later, Schuster et al. (2003) and Yu et al. (2003) generalized the Katz algorithm from 1-D imaging to the theory of multi-dimensional migration of autocorrelograms. In 2001, Schuster generalized the daylight imaging method to be valid for a wide range of waves and source and receiver geometries, including VSP, CDP and transmission experiments. Schuster (1999, 2004), Schuster and Rickett (2000), and Schuster (2001) extended the notion of passive seismic

imaging and daylight imaging to what they named as seismic interferometric imaging. The idea is to backproject crosscorrelograms and enforce an imaging condition that estimates a reflectivity-like function. This theory avoids the restriction that there must be a random distribution of sources below the layers, allows the use of many types of events besides the ghost reflection, and can be used for source location estimation. In 2003, Wapenaar et al mathematically proved Claerbout's 1-D imaging theorem for autocorrelation to 3-D models and random distributions of sources below the layers. Another recent technique, namely virtual source imaging (Calvert et al., 2004; Bakulin and Calvert, 2004). is also a type of daylight imaging, but with a different configuration. In virtual source imaging, the random sources are distributed on the surface, and geophones are placed in a horizontal (or deviated) well that is below the overburden.

An interesting application of interferometry is the theory of coda wave interferometry (Snieder et al., 2002, 2004) developed to determine the nonlinear temperature dependence of the seismic velocity in granite. In this method, a seismogram recorded at an early time is crosscorrelated with the seismogram recorded later in time when the temperature of the rock sample has changed. Temperature changes lead to mechanical changes in the rock, which amplify changes in the scattering coda.

1.1.2 Basic Principles

To illustrate some key principles of seismic interferometry, consider the inverse vertical seismic profile (IVSP) experiment in Figure 1.1, where the seismic source is buried at location $\mathbf{s}$ and receivers are at positions $\mathbf{A'}$ and $\mathbf{B}$ on the earth's free surface. The source excites an upgoing wave that gets reflected at the earth's free surface to generate a ghost reflection. Traces are digitally recorded at the earth's free surface by seismometers at $\mathbf{A'}$ and $\mathbf{B}$; the recorded arrivals consist of direct and ghost reflections and, for pedagogical convenience, we neglect primary reflections (they can be separated by a $f-k$ filtering of VSP data) and smaller energy terms that are 2nd-order or higher in the reflection coefficient R:

$$\tilde{d}(\ \mathbf{s},\ \mathbf{A'}) = W(\omega)[\overbrace{e^{i\omega\tau_{sA'}}}^{dA'} + \overbrace{Re^{i\omega(\tau_{sA''}+\tau_{A''r'}+\tau_{r'A'})}}^{gA'}]; \tag{1.1}$$

$$\tilde{d}(\ \mathbf{s},\ \mathbf{B}) = W(\omega)[\overbrace{e^{i\omega\tau_{sB}}}^{dB} + \overbrace{Re^{i\omega(\tau_{sA}+\tau_{Ar}+\tau_{rB})}}^{gB}], \tag{1.2}$$

where $\mathbf{A}''$ is the specular bounce point at the free surface for the ghost reflection recorded at $\mathbf{A}'$, τ_{ij} is the propagation time between the points i and j, R is the reflection coefficient associated with the sediment interface, and ω is the angular frequency of the harmonic wave. The specular reflection points at the sediment interface are denoted as r and r'; the symbols dA' and gA' (dB and gB) denote the direct and ghost arrivals recorded at $\mathbf{A}'$ ($\mathbf{B}$), and $W(\omega)$ is the spectrum of the source wavelet that also contains timing and mispositioning errors at the source well location we denote as statics.

The so-called "seismic interferogram" is the temporal correlation of the trace at $\mathbf{A}'$ with the one at $\mathbf{B}$, or in the frequency domain is the product

$$\begin{aligned} \phi(\ \mathbf{A}',\ \mathbf{B}) = \tilde{d}(\ \mathbf{s},\ \mathbf{B})\tilde{d}(\ \mathbf{s},\ \mathbf{A}')^* &= gB \cdot dA'^* + \overbrace{dB \cdot gA'^* + dB \cdot dA'^* + gB \cdot gA'^*}^{other\ terms}, \\ &= |W(\omega)|^2 Re^{i\omega(\tau_{sA}+\tau_{Ar}+\tau_{rB}-\tau_{sA'})} + o.t., \end{aligned} \tag{1.3}$$

where $o.t.$ denotes "other terms". These other terms will be ignored because we are mostly interested in the primary reflections for imaging; synthetic and field data applications show that the other terms mostly cancel upon imaging (i.e., migration) and stacking of many migrated shot gathers of traces.

If we were lucky and planted the geophone at the specular bounce point of the ghost reflection (i.e., $\mathbf{A}' = \mathbf{A}$) then equation 1.3 reduces to

$$\phi(\mathbf{A},\mathbf{B}) = |W(\omega)|^2 Re^{i\omega(\tau_{Ar}+\tau_{rB})} + o.t.. \tag{1.4}$$

To rely less on luck, we make up for any planting errors by summing the correlograms in equation 1.3 over all buried source positions:

$$\Phi(\ \mathbf{A},\ \mathbf{B}) = \sum_s \phi(\ \mathbf{A},\ \mathbf{B}) \approx |W(\omega)|^2 \sum_s Re^{i\omega(\tau_{sA}-\tau_{sA'}+\tau_{Ar}+\tau_{rB})} + o.t., \tag{1.5}$$

where many buried sources are assumed to be distributed over a large subsurface area. At high frequencies (in the range of useful seismic frequencies) and fixed $\mathbf{A}$ and $\mathbf{B}$ locations, stationary phase theory says that the dominant contribution to this summation will be the source position $\mathbf{s}^*$ that generates a specular ghost reflection point at position $\mathbf{A}$ on the free surface. Thus, $\phi(\ \mathbf{A},\ \mathbf{B}) \approx |W(\omega)|^2 Re^{i\omega(\tau_{sA}-\tau_{sA'}+\tau_{Ar}+\tau_{rB})}$ in equation 1.5 reduces to an event with the same kinematics as the primary reflection in equation 1.4.

Successful applications of seismic interferometry are summarized in Figure 1.2. These include: migration of VSP ghosts, salt flank imaging, salt flank imaging by P-S converted waves (Xiao et al., 2005), migration of CDP multiples, and migration of diffraction

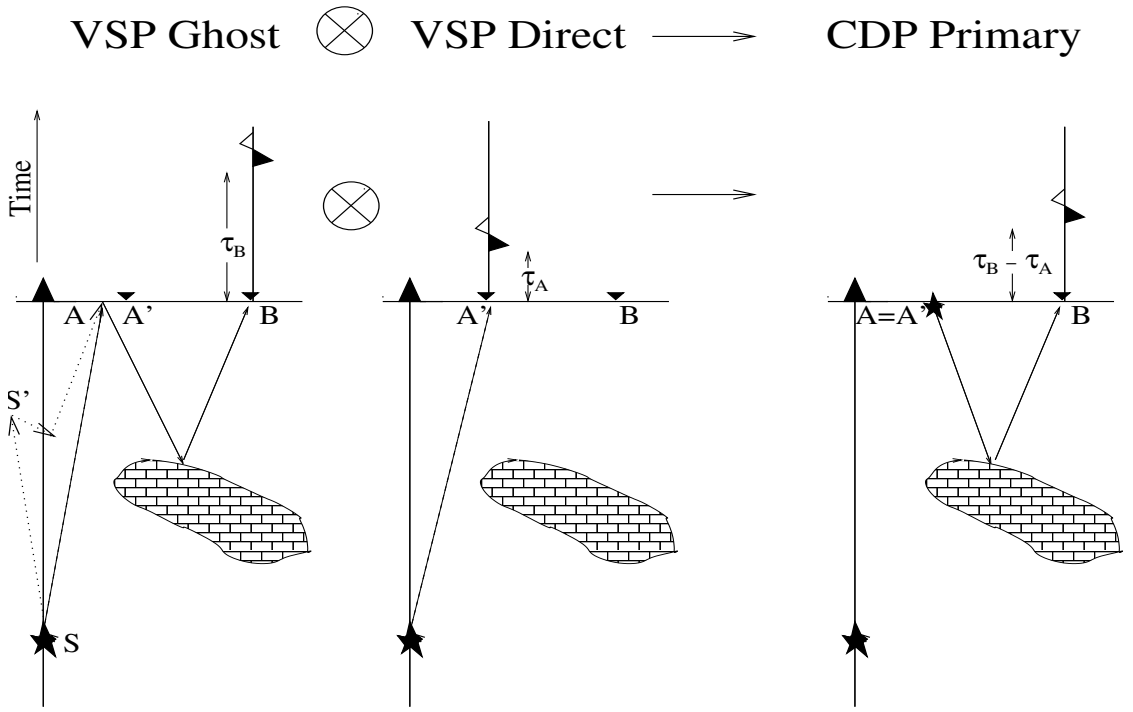

Figure 1.1. Correlation of a ghost arrival at B (dashed-solid ray) with a direct arrival at A' (dashed ray) yields the redatumed CDP data. The ray SS'A is an upgoing pegleg arrival acting as another "direct" wave that generates a ghost reflection.

multiples. More applications are possible, such as HSP (Horizontal Seismic Profile) imaging. This thesis will mainly focus on interferometric 3D migration of VSP multiples and VSP primary reflections.

1.1.3 Benefits and Liabilities

Migration of the correlograms in equation 1.5 is known as interferometric imaging. There are several important benefits of interferometric imaging compared to standard migration:

- **Better image resolution because sources and receivers are redatumed to be closer to the target body.** Equation 1.4 (or asymptotically equation 1.5) is kinematically equivalent to a primary reflection excited by a source at **A** and recorded at **B**, as shown in Figures 1.1. We denote this virtual transformation of VSP data to land data as VSP-to-CDP redatuming, where CDP denotes common-depth-point. This is a desirable transformation because now the source is closer to the target reflector, hence better resolution of its properties is possible. Other examples are shown in Figures 1.2b-c where the distortion due to the overburden velocity is eliminated in redatuming data so that the surface source is virtually relocated to deep locations along the well (Calvert et al., 2004; Xiao et al., 2005), i.e., VSP data transformed to single well imaging (SWI) data.

- **Passive seismic imaging.** The first term of the correlogram $\phi(\mathbf{A},\mathbf{B})$ in equation 1.4 is independent of the source phase, the position of the seismic source along **sA** and, the seismic properties of the uninteresting medium below the reflector denoted by R. This means that the source location, the medium below the reflector and the source's initiation time do not need to be known in order to image the reflector geometry from $\phi(\mathbf{A},\mathbf{B})$. Thus, one of the uses of seismic interferometry is for passive seismic imaging (Rickett and Claerbout, 1999; Draganov et al., 2004) where geophones passively record the earth's natural vibrations over a long period of time. Yu and Schuster (2001) successfully applied seismic interferometry to drill-bit seismic data.

- **Source statics elimination.** Timing errors (known as statics) due to mispositioning of the buried source or incorrect excitation times are not present in $\phi(\mathbf{A},\mathbf{B})$

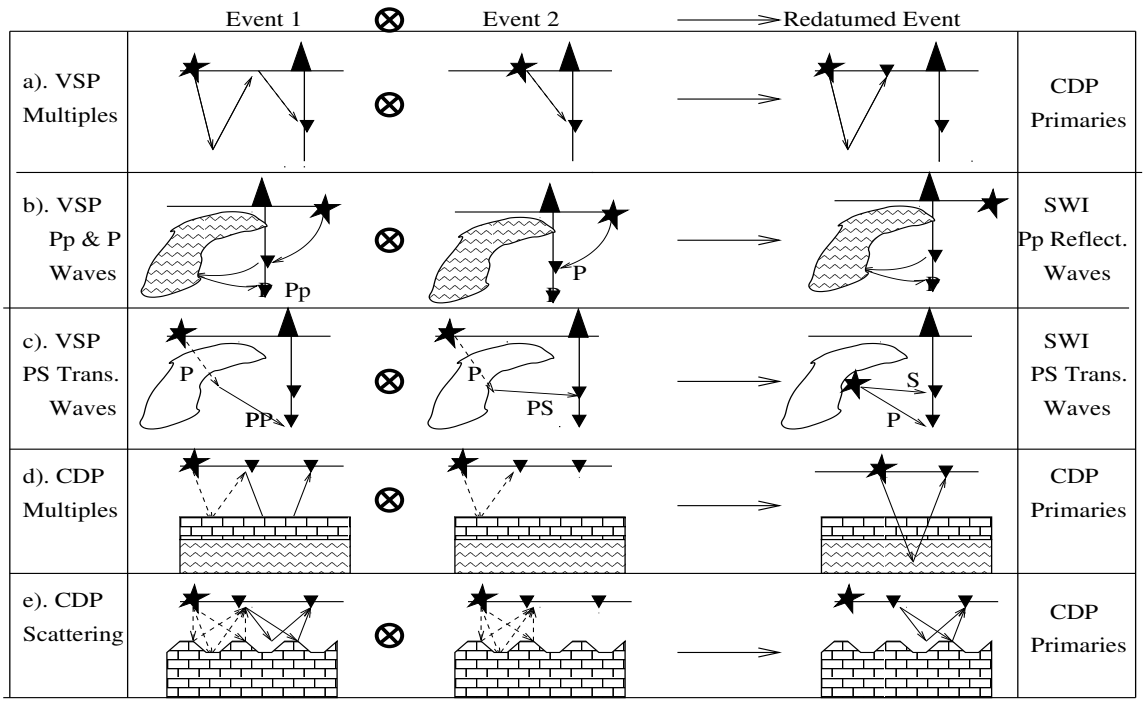

Figure 1.2. Table of scattering diagrams for different applications of seismic interferometry. Leftmost column denotes the input data and rightmost column indicates the type of data after interferometric redatuming.

because their phases were canceled in the correlation of $W(\omega)$. Thus, source-statics corrections are not needed compared to the mandatory statics corrections used for standard VSP data.

- **Super resolution.** Energy associated with the pegleg multiples are transformed to be primary reflection energy, as illustrated in Figure 1.2e. The transformation of all such "pegleg" energy into primary reflection energy increases the signal-to-noise ratio of the virtual primary reflection, but can also contribute to a wider diversity of incidence angles leading to super resolution in the reflectivity image. Such an example in shown in Figure 1.3.

- **Robust imaging.** Because of the insensitivity to distortion by the overburden and statics, IM can sometimes more robustly image the subsurface compared to standard seismic imaging. An example is shown in Figure 1.4. This kind of example is also shown in virtual source imaging (Bakulin and Calvert, 2004), but virtual source imaging is a type of IM.

A key problem with seismic interferometry is that other events, labeled as *other terms* in equation 1.3 and denoted as *virtual multiples* in Schuster (2001), can be coherently imaged by the migration operator and appear as coherent noise. Some partial remedies are 1). filter out unwanted events prior to crosscorrelation, and 2). deconvolution (Calvert et al., 2004; Muijis et al., 2005). Another important problem is that multiples suffer more geometrical spreading and attenuation losses compared to primary reflections.

1.2 Wave-equation Interferometric Migration (WEIM)

Untill now, most IM methods have been implemented by applying Kirchhoff migration to the crosscorrelograms. In many cases, Kirchhoff migration is more efficient than wave-equation migration. However, when the number of sources is many more than the number of receivers, this convention can be reversed because of the computational savings in ray tracing costs and storage for time tables in wave-equation migration. This is the situation for migration of 3D VSP multiples because in a typical 3D VSP walkaway survey, there are usually thousands of sources on the surface, but very few geophones in the well. In the next chapters, WEIM will be developed from the conventional IM method, and applied to 3D migration of VSP multiples and VSP salt flank imaging. The benefits are that

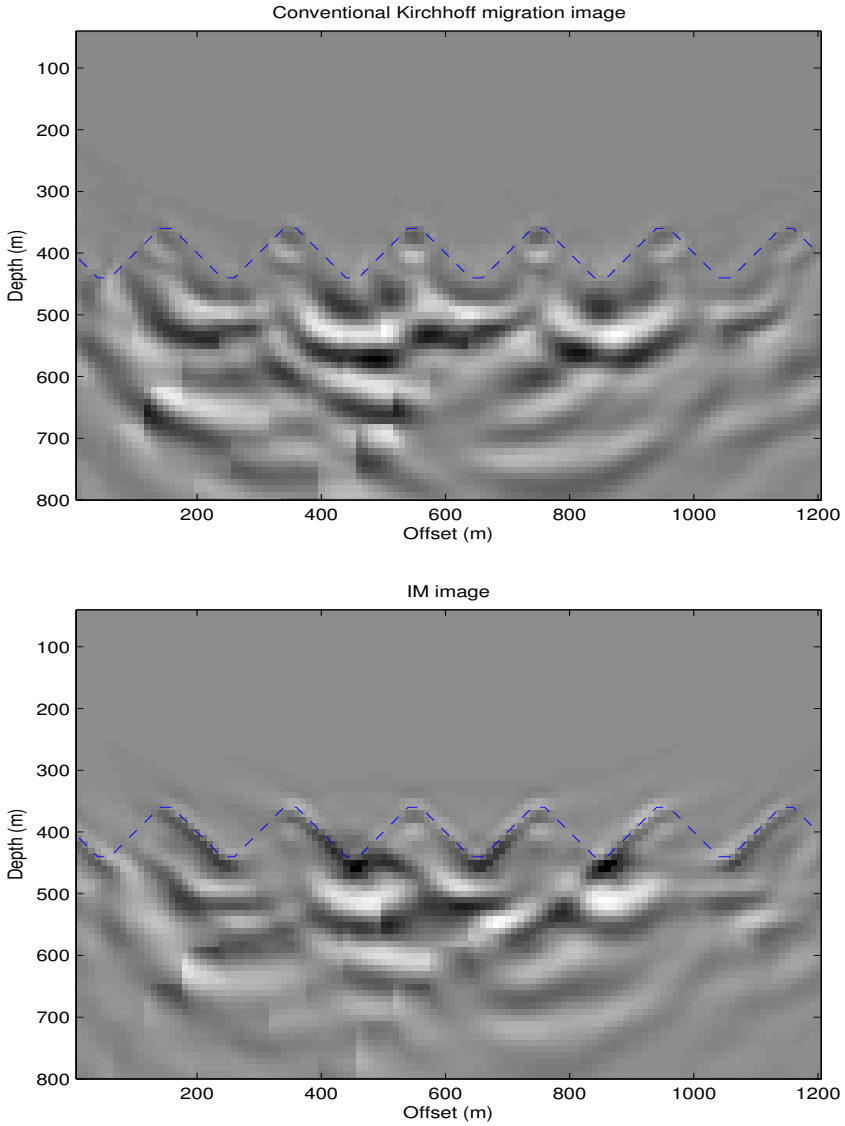

Figure 1.3. (Top) A migration image after conventional Kirchhoff migration of CDP primaries in 120 shot gathers, each with 120 geophones evenly distributed on the surface. The undulating sea floor (denoted by a dashed line) is not clearly imaged because the dominant seismic wavelength in water is about 150 m in this example, which is much longer than the fluctuation wavelength of the sea floor (50 m in depth). (Bottom) The migration image after IM. The undulating sea floor is now better imaged because of a wider diversity of incidence angles associated with diffraction multiples. This could be important for estimating the rugose geometry of a salt interface.

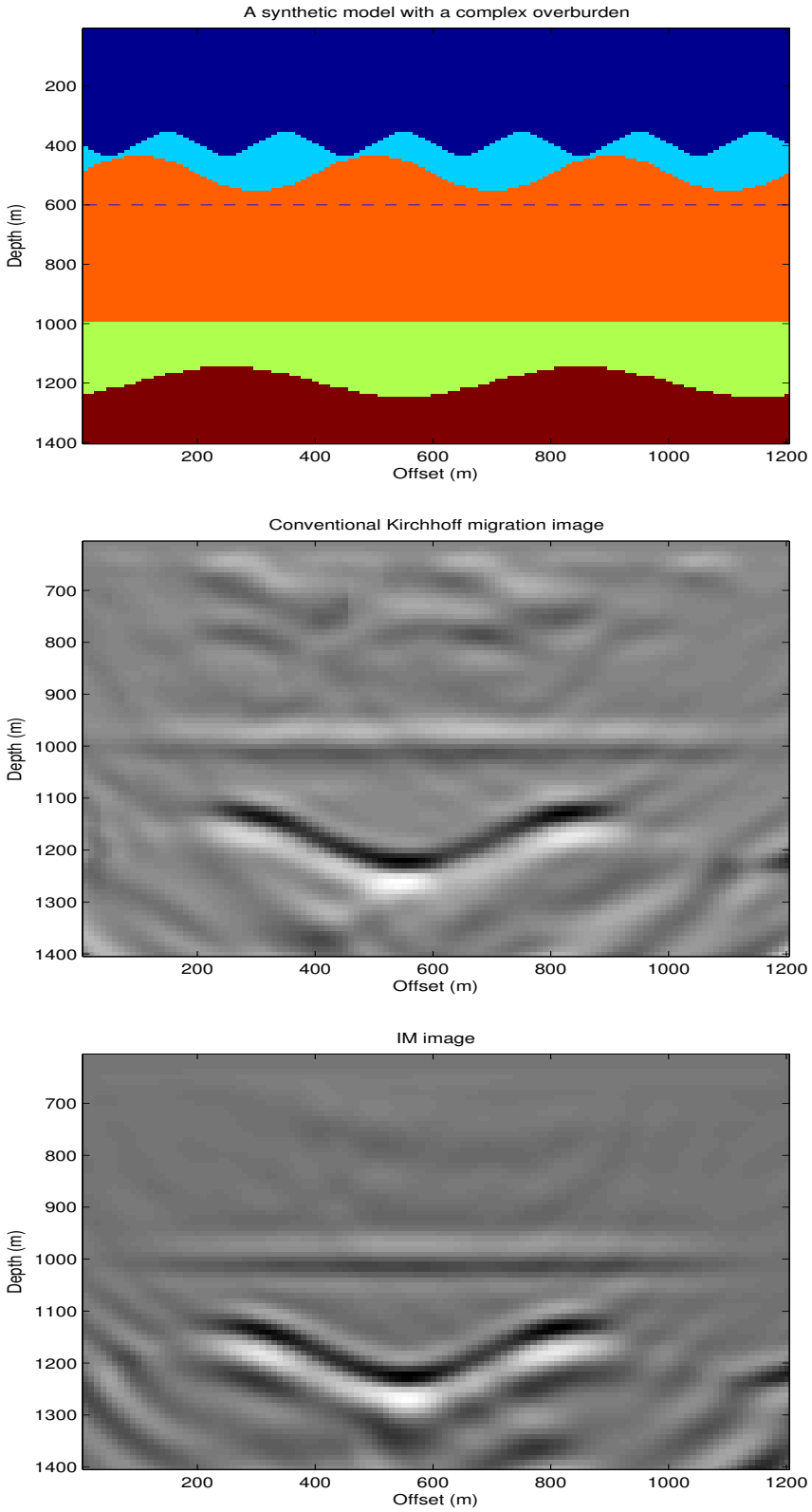

Figure 1.4. (Top) A synthetic horizontal well experiment. There are 100 shots evenly deployed on the surface, and 100 geophones evenly placed in the horizontal well (dashed line) below a complex overburden. The area below the well is the target zone. (Middle) This is the result after conventional Kirchhoff migration. Even with the exact velocity model, the migration image of the target area is not clean because of distortion due to the overburden. (Bottom) This is the result after IM. Without the overburden in migration, it is more efficient, and the result is more accurate.

WEIM is computationally more efficient than standard IM, and in theory, more accurate.

1.3 Technical Contributions in This Dissertation

There are two major technical contributions in this dissertation:

1. The WEIM is developed for the efficient migration of 3D VSP multiples. For each receiver gather of 3D VSP data, WEIM requires the calculation of only one 3D receiver gather of travel times and one 3D wavefield extrapolation to migrate the 3D VSP free-surface multiples. Compared to the expensive acquisition and processing costs of a 3D CDP survey, the tremendous efficiency in obtaining a 3D subsurface image volume by migration of 3D VSP free-surface multiples suggests that a 3D VSP survey can also serve as a cost effective 4D monitoring tool for some oil fields.

2. Expanded the application regime of seismic interferometry. Conventional surface seismic data are not good at imaging vertical subsurface structures, such as salt flanks. VSP salt flank imaging by interferometric methods is not only efficient and but also effective in practice because a large chunk of overburden is bypassed.

CHAPTER 2

3D WEIM OF 3D VSP MULTIPLES

A 3D wave-equation interferometric migration (WEIM) method is developed for efficiently migrating multiples in 3D VSP data. With WEIM, for each receiver gather of 3D VSP data, only one 3D receiver gather of travel times and one 3D wavefield extrapolation need to be calculated for the migration of free-surface multiples. Compared to the expensive acquisition and processing costs of a 3D surface seismic survey, the tremendous efficiency in obtaining a 3D subsurface image volume by migration of free-surface multiples suggests that a 3D VSP survey can also serve as a cost effective 4D monitoring tool for some oil fields. However, the low fold image from the migration of a handful of receiver gathers can lead to troublesome acquisition footprints and low S/N ratios.

2.1 Introduction

It is well known that migration of VSP primaries has a limited imaging area that is roughly a cone-shaped zone with the cone tip centered at the shallowest geophone in the well (this will be demonstrated by the following synthetic experiment). To overcome this problem, Yu and Schuster (2001, 2006) and Jiang et al. (2005) demonstrated that migration of VSP free-surface multiples has a much wider imaging area in the horizontal direction, and most importantly the area above the geophones is also imaged. Their field data applications showed that migration of VSP multiples can achieve an imaging area similar to that of a small CDP survey around the well. A physical explanation for this success is that the first-order VSP free-surface multiples have only one extra reflection point compared to the CDP primaries (see Figure 2.1), and that this reflection point is at the free surface which, in the marine case, has a -1 reflection coefficient. In marine seismic data, VSP free-surface multiples are usually strong events, and if the water depth is deep enough, they are naturally well separated from the earlier strong VSP primaries. These characteristics make marine VSP free-surface multiples very useful for imaging the subsurface.

A number of field data examples have been presented (Jiang et al., 2005; Jiang, 2006; Yu and Schuster, 2001 and 2006) that demonstrate the effectiveness of multiple migration applied to VSP data. Comparison to CDP records demonstrated the accuracy of this method. However, until now, there are no published reports about the 3D migration of VSP multiples in 3D field data. There are synthetic tests (Jiang, 2006) that demonstrate the effectiveness of 3D IM of VSP data, but the crucial step of demonstrating its effectiveness with field data is non-existent.

In this paper, I develop a wave-equation interferometric method to migrate the free-surface multiples in 3D VSP data. Results show a plausible image of the subsurface that reveals a variety of reflections including a salt body. Image gathers show flat events which indicate the accuracy of this image. One of the important implications of the WEIM method is that, in principle, it can be efficiently applied to time-lapse VSP data to monitor the extraction pressure of a developed oil field. Ideally, time-lapse 4D monitoring of an oil field by interferometric migration of multiples can possibly be much less expensive that of the traditional surface survey.

This paper is composed into 3 sections. In the first section, the theory of WEIM is derived from the conventional IM method. The second section shows the results of a synthetic 2D VSP experiment that tests this method, and compares it to a conventional image obtained from primary reflections in VSP data. After that, this method is applied to a field 3D VSP dataset. The results confirm that this method is efficient, and an image volume similar to that of a small CDP survey around the well is obtained. The last section provides a summary and conclusion.

2.2 Theory

For pedagogical clarity, we will discuss the IVSP example shown in Figure 2.1, with the understanding that VSP data can be transformed to be IVSP data by reciprocity (Aki and Richard, 2002). Figure 2.1 shows the raypath of an IVSP free-surface multiple event. The IM of such multiples can be carried out in two steps (Yu and Schuster, 2006). First, the two IVSP seismograms at $\mathbf{g}_1$ and $\mathbf{g}_2$ are crosscorrelated, and summed over all buried sources:

$$\phi(\mathbf{g}_1, \mathbf{g}_2, t) = \sum_s d(\mathbf{g}_1, \mathbf{s}, t) \otimes d(\mathbf{g}_2, \mathbf{s}, t), \tag{2.1}$$

where $\mathbf{g}_1, \mathbf{g}_2 \in B_0$ represent two geophone positions on the free surface, d represents the seismogram, ϕ defines the crosscorrelogram between two seismograms, and $\otimes$ denotes the

crosscorrelation operation.

Equation 2.1 is exactly the same as for interferometric imaging (Schuster 2001; Yu and Schuster 2001), and is similar to that in virtual source imaging (Calvert et al., 2004; Bakulin and Calvert, 2004). One difference is that in virtual source imaging, the source deconvolution is required. However, in IM, this restriction if lifted. As in daylight imaging, this trace crosscorrelogram can be migrated as if it is the reflection recorded at $\mathbf{g}_2$ with an impulsive source located at $\mathbf{g}_1$. In the frequency domain, the migration image $m(\mathbf{x}, \omega)$ obtained from a single pair of correlated traces is:

$$m(\mathbf{x}, \omega) = \Phi(\mathbf{g}_1, \mathbf{g}_2, \omega) e^{-i\omega(\tau_{xg_1} + \tau_{xg_2})}, \tag{2.2}$$

where $\mathbf{x}$ is the image point, $\tau_{gg'}$ is the traveltime for waves to propagate from g to g', Φ is the spectrum of ϕ, ω is the angular frequency, and $i = \sqrt{-1}$. The stacked migration image over all $\mathbf{g}_1$ and $\mathbf{g}_2$ locations on the free surface is:

$$M(\mathbf{x}, \omega) = \sum_{\mathbf{g}_2 \in B_0} \sum_{\mathbf{g}_1 \in B_0} \Phi(\mathbf{g}_1, \mathbf{g}_2, \omega) e^{-i\omega(\tau_{xg_1} + \tau_{xg_2})} dg_1 dg_2. \tag{2.3}$$

Note, the summation over all $\mathbf{g}_1$ and $\mathbf{g}_2$ on the free surface means that all specular reflections are included, but non-specular reflections are also included. One advantage of interferometry is that we do not need to select these specular reflections for migration. For computational convenience, the geophone distribution on the surface should be uniform and have enough small spacing to avoid the possible aliasing problem.

From equation 2.3, we can see the traveltime from the source $\mathbf{s}$ to $\mathbf{g}_1$ does not need to be computed. This shows that IM can be used for passive imaging where the source location and source initial time does not need to be known for imaging. It is also obvious that migration of the above crosscorrelograms is similar to the migration of CDP primaries, and indeed, the velocity estimation errors they experience in practice and their resulting imaging areas are also similar.

A Kirchhoff implementation of equation 2.3 requires the calculation of traveltime fields for virtual sources located at all geophone positions on B_0, and this can be quite costly for 3D migration of IVSP data as mentioned above. So we need to find out a more efficient way to calculate the migration image.

This can be accomplished by replacing Φ by $\sum_{\mathbf{s}} D^*(\mathbf{g}_1, \mathbf{s}, \omega) D(\mathbf{g}_2, \mathbf{s}, \omega)$ (D is the spectrum of d, and the superscript * denotes conjugate) in equation 2.3, and reorganizing the equation as:

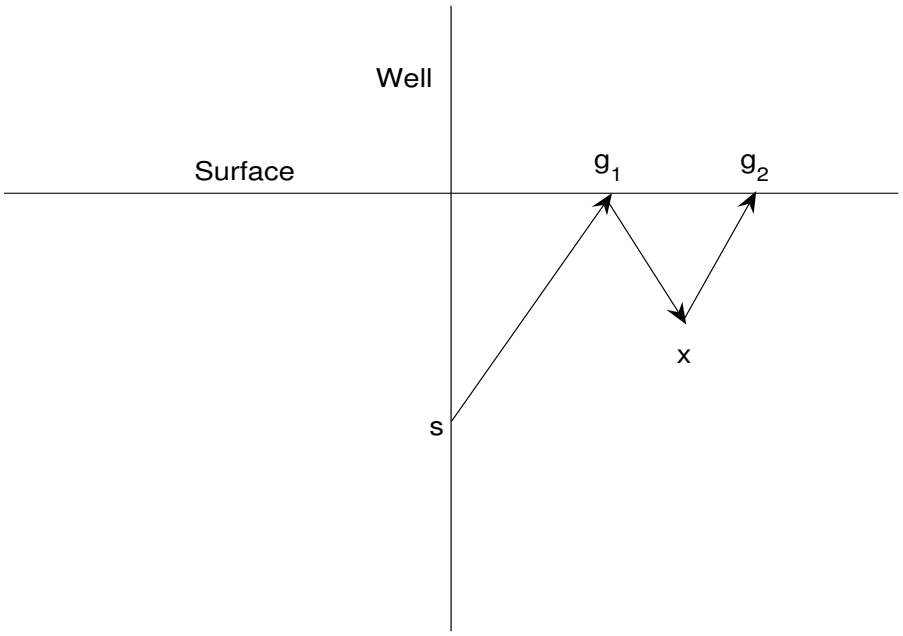

Figure 2.1. A ray for an IVSP free-surface multiple. By reciprocity, the equivalent VSP raypath starts at the surface source at g_2, and ends at the well position s. We will show that migration of this IVSP free-surface multiple will be kinematically equivalent to the migration of a primary reflection generated by a source at g_1 position, and a geophone at g_2 position.

$$
\begin{aligned}
M(\mathbf{x},\omega) &= \sum_s [\sum_{\mathbf{g}_1 \in B_0} D(\mathbf{g}_1,\mathbf{s},\omega) e^{i\omega\tau_{xg_1}}\, dg_1]^* \\
&\times \sum_{\mathbf{g}_2 \in B_0} D(\mathbf{g}_2,\mathbf{s},\omega) e^{-i\omega\tau_{xg_2}}\, dg_2 \\
&= \sum_s [F(\mathbf{x},\mathbf{s},\omega)]^* B(\mathbf{x},\mathbf{s},\omega), \qquad (2.4)
\end{aligned}
$$

where $F(\mathbf{x},\mathbf{s},\omega)$ and $B(\mathbf{x},\mathbf{s},\omega)$ means forward and backward extrapolated wavefield spectra at the image point respectively (note, amplitude factors are not taken into account here, but can be accounted for if needed). Equation 2.4 is the basic formula for WEIM, and is identical to that for reverse-time migration (RTM) (Baysal et al., 1983; McMechan, 1983), except in RTM, the F is modeled for a source at the actual point source, and both of the forward and backward wavefield extrapolations use two-way wavefield extrapolators (e.g. finite-difference methods). In WEIM, the F is forward extrapolated directly from the recorded seismic data, and both of the forward and backward wavefield extrapolations can use either one-way wavefield extrapolators (e.g. phase-shift methods) or two-way wavefield extrapolators.

If both of the forward and backward wavefield extrapolations are computed by wave-equation methods, WEIM does not require ray tracing at all (hence no time table is stored). But, this is not the most efficient strategy. In most IVSP experiments, the direct wave usually is by far the strongest event. In this case, we can replace the forward wavefield extrapolation in equation 2.4 by a ray tracing exercise:

$$
M(\mathbf{x},\omega) = \sum_s e^{-i\omega\tilde{\tau}_{sx}} B(\mathbf{x},\mathbf{s},\omega), \qquad (2.5)
$$

where $\tilde{\tau}_{sx}$ is the time calculated by ray tracing for energy to propagate from $\mathbf{s}$ to $\mathbf{x}$, so that the computational efficiency is improved. In Equation 2.5, $\tilde{\tau}_{sx} = \tilde{\tau}_{sg_1} + \tau_{g_1x}$ is the arrival time of the IVSP direct wave after reflection from the free surface. In order to compute this traveltime, we can first pick (this can be easily done by an auto-pick program) the direct arrival time $\tilde{\tau}_{sg_1}$ from the data, and then insert it into a ray tracer; the downgoing traveltime τ_{g_1x} from $\mathbf{g}_1$ to the trial image point $\mathbf{x}$ is computed by ray tracing. Comparing to the conventional point-source ray tracing (Qin et al., 1992), this kind of ray tracing is as efficient as the conventional point-source ray tracing. The computed traveltime will be the arrival time of the IVSP direct wave after reflection from the free surface. The advantage of this ray tracing is obvious: the ray tracing from the actual point source to the surface is saved just by picking. This is not only efficient because of the computational

savings in ray tracing, but also the source-side statics are also eliminated. Schuster's (2003) semi-natural migration has the same advantage.

In equation 2.5, it is preferred to have only the IVSP free-surface multiples to be backward extrapolated. In order to separate the IVSP free-surface multiples, an $f-k$ filter is usually applied to the IVSP receiver gathers. The resulting downgoing wavefield (beside the IVSP direct wave) is usually assumed to be mainly the IVSP free-surface multiples. In marine IVSP data, if the water depth is deep enough, IVSP free-surface multiples are usually well separated from the earlier strong IVSP primaries, so that the above $f-k$ filtering is unnecessary if we start constructing the migration image just above the water bottom. This is shown in the following synthetic and real data examples.

2.3 Numerical examples

In the following two subsections, a 2D synthetic and a 3D field VSP dataset are used to test WEIM for migration of VSP free-surface multiples.

2.3.1 2D Synthetic Experiment

The top left picture of Figure 2.2 shows a synthetic 2D density model used for testing the proposed WEIM method. There are 12 geophones evenly placed in the center well, and 600 shots evenly deployed on the surface (in field surveys, geophones and shots usually are evenly placed for the convenience of acquisition and processing). The VSP data are synthesized by acoustic finite-difference modeling. The top right picture of Figure 2.2 shows a receiver gather of the synthetic VSP data. From it we see, the free-surface multiples start at about 3.5 s, and are well separated from the earlier strong VSP primaries, so that the unfiltered VSP data can be directly input to the migration program (the constructing of migration image starts just above the water bottom). The bottom left picture of Figure 2.2 shows the image after migration of primaries, and the bottom right picture of Figure 2.2 shows the image after migration of free-surface multiples. From it we see, the migration of VSP free-surface multiples indeed has a wider imaging area than that of migration of VSP primaries, and the area above the geophones is also imaged.

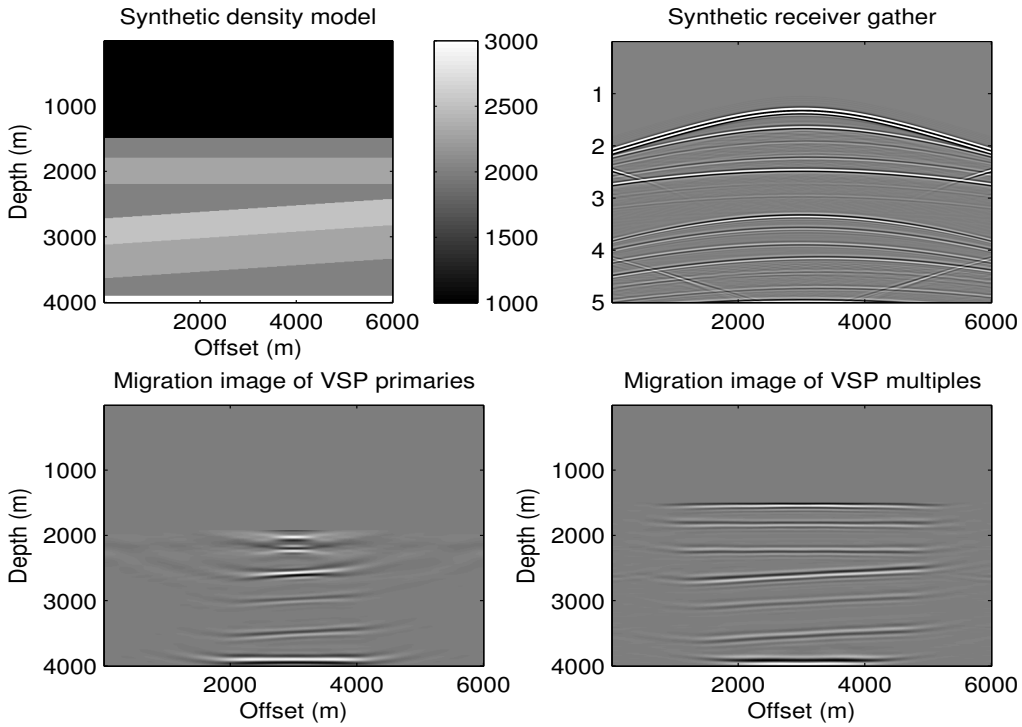

Figure 2.2. (Top left) A synthetic 2D density model with 12 geophones evenly distributed in the center between the depths of 1900 m to 2120 m. There are 600 shots with a 10 m shot interval evenly located on the surface. (Top right) A synthetic common receiver gather of VSP data by finite-difference modeling. From it we see, the VSP free-surface multiples are strong events, and because the water depth is deep enough, they are naturally well separated from the earlier strong VSP primaries. (Bottom left) The image area after migration of VSP primaries is a cone-shaped zone, and the area above the geophones is not imaged. (Bottom right) The image after migration of VSP free-surface multiples. It has a larger imaging area than that after migration of primaries, and most importantly the area above the geophones is now imaged.

2.3.2 3D Field Data Application

Figure 2.3 shows the spiral pattern (an optimal pattern would be a 2D grid with equal spacing in both horizontal directions) of a real shot geometry for a 3D VSP survey conducted by BP in the Gulf of Mexico. Three similar spirals of shots were carried out with a string of twelve 3-component geophones in the center well, but each geophone string is offset by about 180 m for each of the spiral surveys. Only the Z-component traces are used for migration. Figure 2.4 shows a section of the 3D data cube. From it we see, the free-surface multiples are strong events, and well separated from the earlier stronger primaries. The unfiltered VSP data are migrated, and the constructing of migration image starts just above the sea floor (about 2000 m).

Figure 2.5 shows the image after 3D migration of 3D VSP multiples for only one receiver gather. This confirms that an image volume comparable to that of a small 3D CDP survey around the well can be efficiently obtained by WEIM. Figure 2.6 shows a slice of the final stacked migration image over 36 receiver gathers. The corresponding slice of the velocity model is shown in Figure 2.7, and it agrees quite well with the migration image (the salt dome is also well depicted). Figure 2.8 shows a common image gather in which the flat events indicate that the 3D migration is accurate.

The wavefield extrapolator used here is the split-step Fourier method (Stoffa, et al., 1992). The 3D VSP data cube used for migration has the dimension $85 \times 87 \times 6000$ (X, Y, and time samples), and the 3D migration was computed by a Matlab program on a PC. For each receiver gather, it only required about 8 hours for a $85 \times 87 \times 700$ (X, Y, and depth samples) image. This is estimated to be 1000 times faster than a brute implementation of Kirchhoff migration which requires about 300 GB disk memory. The computational efficiency should be even improved if the program is implemented in C or Fortran.

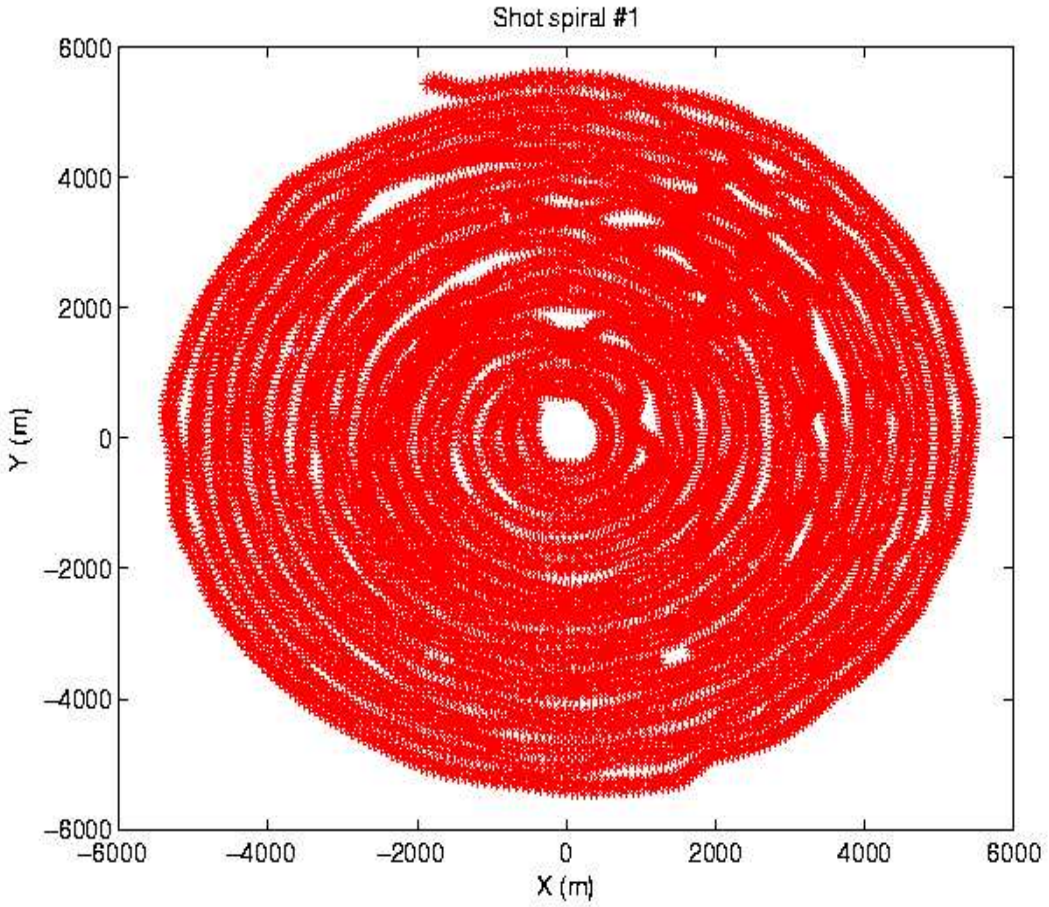

Figure 2.3. Spiral pattern shot geometry for a 3D VSP survey in the Gulf of Mexico. The geophones record data from three such shot spirals and the ensemble of all traces is equivalent to a 36-geophone array with an approximate 15 m geophone spacing, at an average depth of about 5000 m.

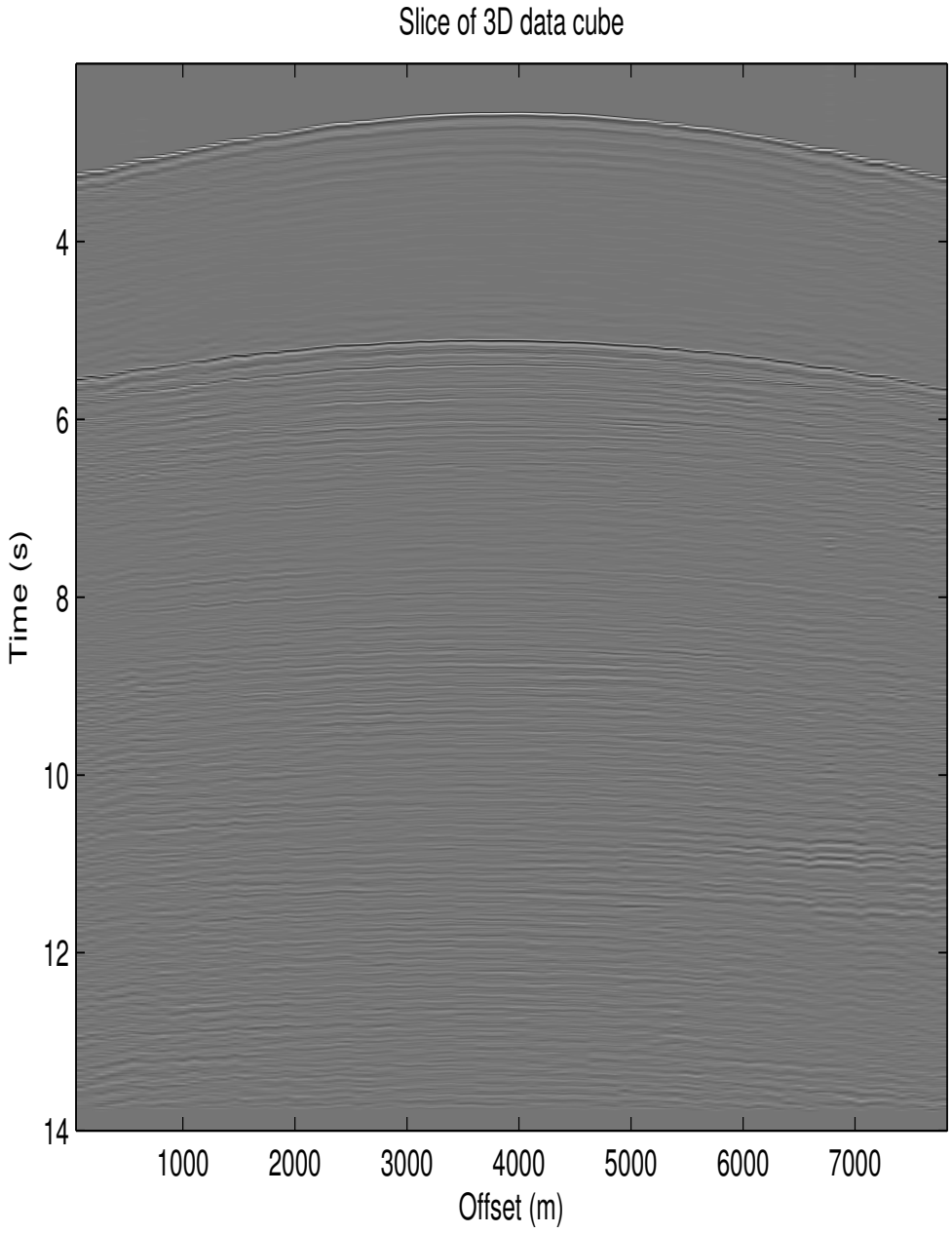

Figure 2.4. A slice of the 3D field data cube. From it we see, the free-surface multiples start at about 5.5 s, and are well separated from the earlier stronger primaries.

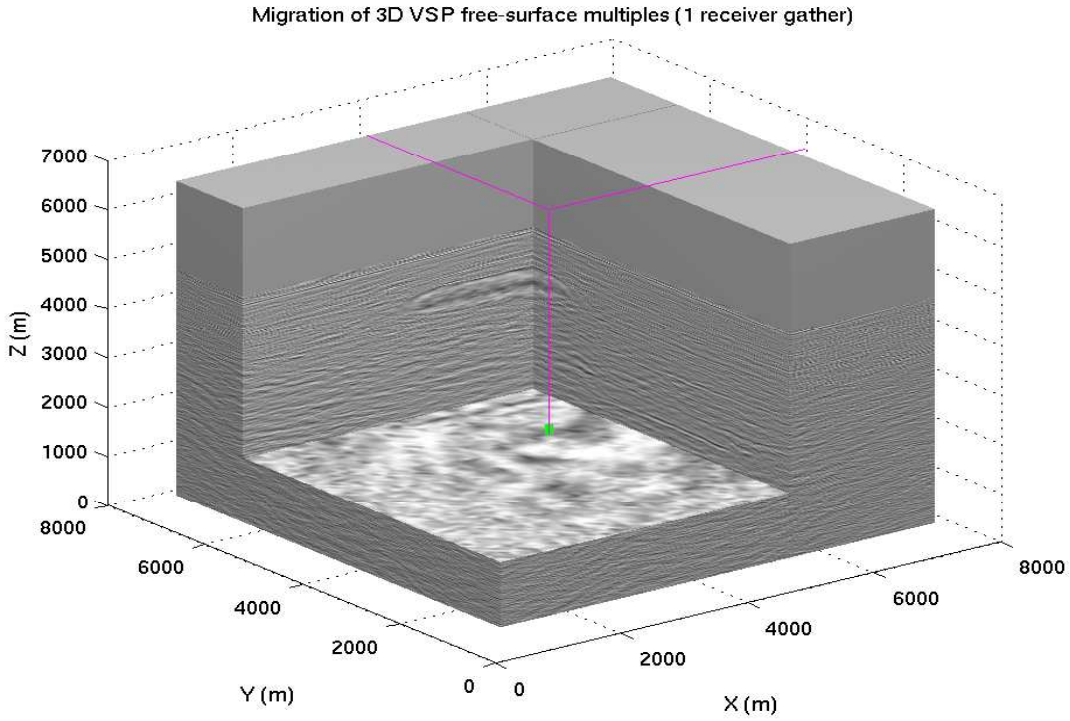

Figure 2.5. The result after 3D migration of VSP free-surface multiples for one receiver gather only. To obtain this result, the calculation of only one 3D receiver gather of traveltimes and only one 3D wavefield extrapolation were required, as compared to a conventional 3D Kirchhoff migration that requires the calculation and storage of 7396 3D shot gathers of traveltimes.

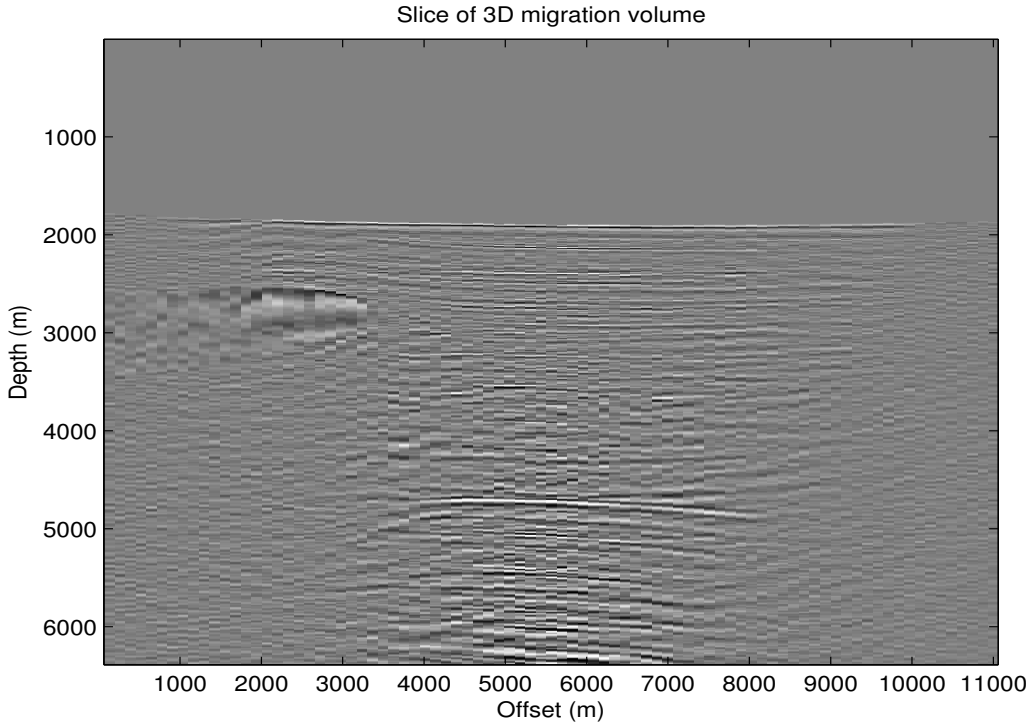

Figure 2.6. A slice of the final stacked 3D migration image for 36 receiver gathers.

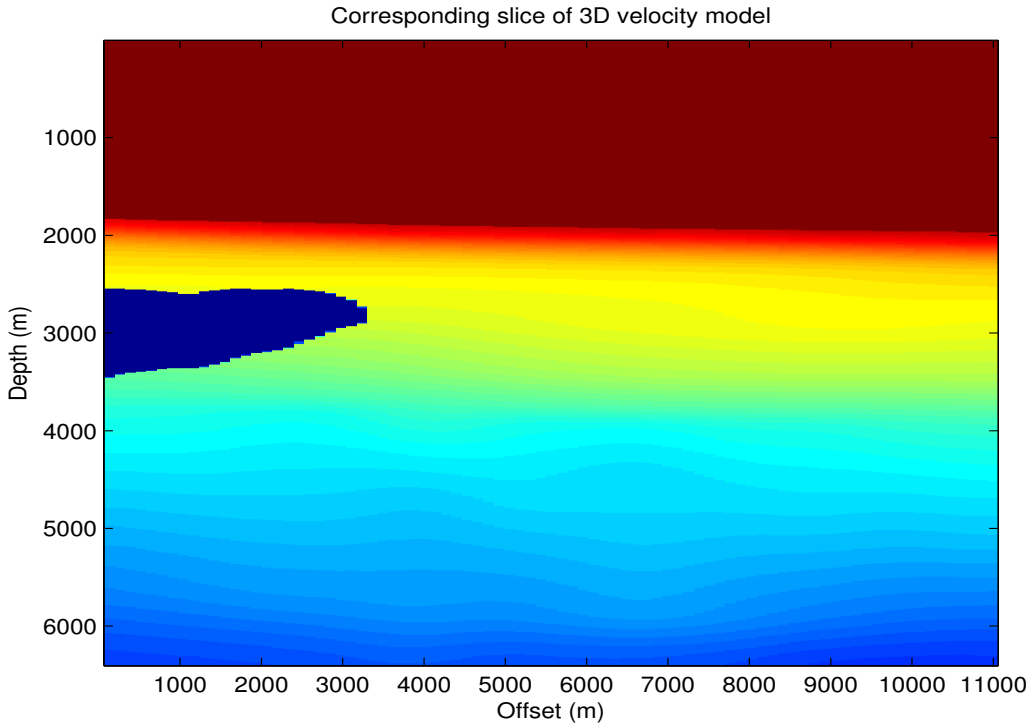

Figure 2.7. The slice of the velocity model corresponding to the migration image shown in Figure 2.6.

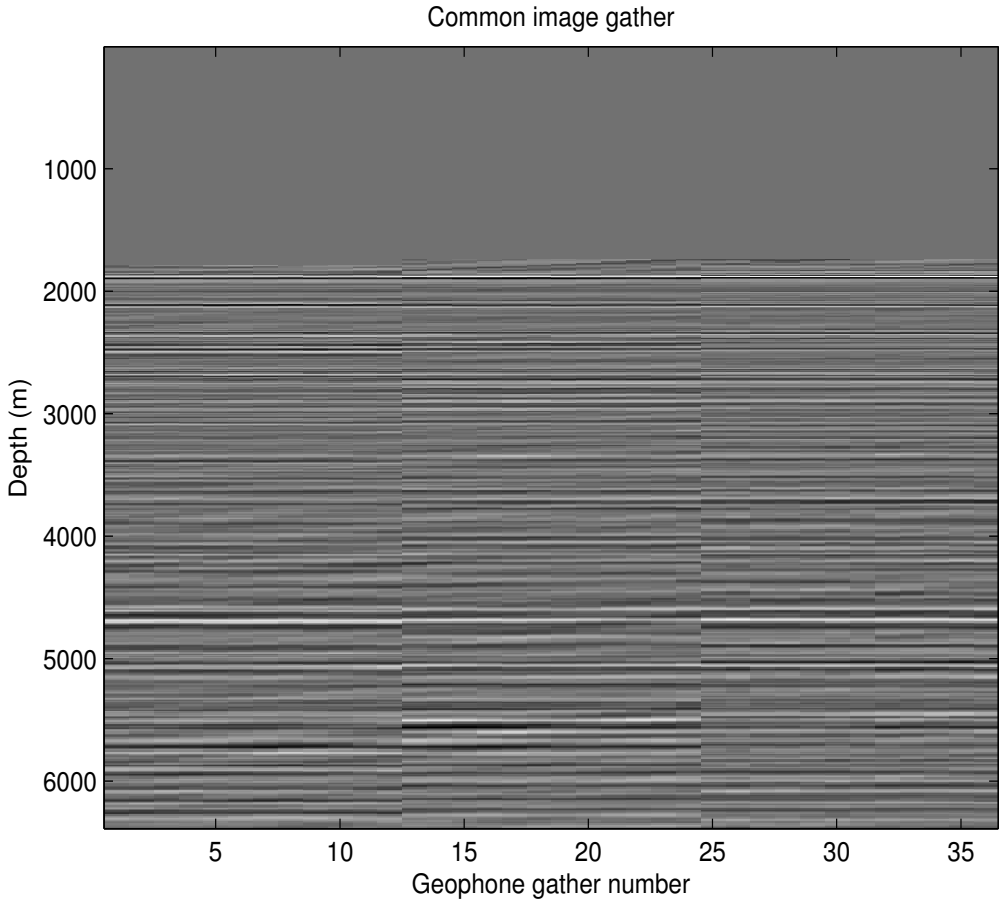

Figure 2.8. A common image gather. From it we can see that all 36 receiver gathers give consistent migration images, and the stack of them improves the S/N ratio of the migration image.

2.4 Conclusion

I have presented an inexpensive procedure for 3D wave-equation migration of 3D VSP free-surface multiples that has an illumination volume comparable to a small 3D CDP survey around the well. Results with synthetic 2D VSP data and field 3D VSP data validate the wide illumination properties of VSP multiple migration, and the flat events (see figure 2.8) in the common image gathers suggest that the migration image is accurate. One important implication of our work is that 3D WEIM of VSP multiples might be an inexpensive means for conducting 4D surveys over some producing oil fields. Only a small number of downhole geophones are needed, inexpensive surface shots can be used, and preexisting production wells can be used for the VSP wells. Drill-bit seismic data can also be used as an IVSP experiment. In some cases, production does not need to be shut down during the VSP survey. However, the low-fold image from the migration of a handful of receiver gathers can lead to troublesome acquisition footprints and low S/N ratios. This is a challenge for future research.

CHAPTER 3

VSP SALT FLANK IMAGING

Wave-equation interferometric migration (WEIM) is proposed for imaging steeply-dipping salt flanks with VSP data. The major advantage of using WEIM for VSP salt flank imaging is that only a local velocity model around the target area is needed. This means that the migration is not only efficient but also accurate in practice because there is no image distortion from erroneous velocity estimation of the overburden. However, a remaining problem is the inability to isolate target reflections in the VSP data, which can result in many artifacts.

3.1 Introduction

Salt flanks act as traps for hydrocarbons, but also act as distorting lenses that severely impair our ability to seismically "see" below salt. It is conjectured that there are huge untapped reservoirs beneath the pervasive salt aprons in the Gulf of Mexico, so that clearly "seeing" below salt is crucial for unlocking these reservoirs (O'Brien and Gray, 1996; Gras et al., 1998; O'Brien et al., 2005; O'Brien 2005).

A traditional method for "seeing" below salt is VSP imaging, where receivers are lowered beneath the salt flanks. For example, salt proximity surveys (Gardner, 1949, Li et al, 2002) are commonly used to delineate the location of salt flanks. This method computes transmitted rays that connect both the source and geophone positions to find the possible salt-sediment interface. The major difficulties of this method are that the final image can be non-unique, and it requires an accurate velocity model outside the salt dome (the homogeneous assumption of the salt dome can also be inaccurate in some cases). Other seismic methods for salt flank imaging include: migration of reflected energy (Whitmore and Lines, 1986), migration of transmitted energy (McMechan et al., 1988), imaging with turning waves (Hale et al., 1992; Hussein et al., 1997), and tomography (Zhang and McMechan, 1994). Recent advances in wavefield continuation numerically datum the surface sources to the geophones and then laterally migrate the horizontal

component VSP data along the horizontal direction (Brandsberg, et al., 2003). All of these methods require a velocity model of the overburden (the area between the surface sources and the geophones along the well), and an erroneous estimation of the overburden velocity will introduce errors into the final salt flank image.

In order to bypass the overburden problem, Willis et al., (2006) proposed an auto-correlation migration method for VSP salt flank imaging. They were able to image the salt flank with only a local velocity model, but the image has some artifacts with the synthetic test. A related work is by Hornby et al. (2006) who showed the possibility of imaging salt flanks by interferometric methods. Here WEIM is introduced for VSP salt flank imaging, and produces a clear salt flank image for synthetic VSP data. The results also show that the salt flank can be imaged by only one shot gather of VSP data, but more shot gathers are needed to enhance the S/N ratio. For field data applications, VSP experiments are usually conducted with a single well, so inaccurate imaging can result from out-of-plane 3D waves.

This chapter is organized in the following way: the first section outlines the theory for VSP salt flank imaging by WEIM. Then a synthetic experiment is conducted to test this method. I carried out a satisfactory application to field VSP data, while working for BP in last summer, but they will not release the results for the time being. A brief conclusion is given at the end.

3.2 Theory

Figure 3.1 shows how the VSP salt flank imaging by WEIM is equivalent to the WEIM of VSP free-surface multiples described in the previous chapter. If we rotate Figure 3.1 by 90^o, then the ray diagram $\overline{\mathbf{s'g}_1\mathbf{g}_2}$ will be the same as $\overline{\mathbf{sg}_1\mathbf{g}_2}$ in Figure 2.1. Thus, the equation for WEIM of salt flank imaging is the same as WEIM of VSP free-surface multiples:

$$M(\mathbf{x},\omega) = \sum_s e^{-i\omega\tilde{\tau}_{s'_x}} B(\mathbf{x},\mathbf{s}',\omega). \tag{3.1}$$

Here, the wavefield extrapolation of $B(\mathbf{x},\mathbf{s}',\omega)$ is along the horizontal direction, and $\tilde{\tau}_{s'_x} = \tilde{\tau}_{s'g_1} + \tau_{g_1x}$ is computed by a line-source ray tracer, where the direct arrival $\tau_{s'g_1}$ is picked from the data. With interferometric methods, the traveltime for waves to propagate from $\mathbf{s}$ to $\mathbf{g}_1$ does not need to be known (this is why we can assume the actual

source $\mathbf{s}$ is at the position of $\mathbf{s}'$), so that a huge chunk of the overburden between $\mathbf{s}$ and $\mathbf{g}_1$ is ignored during migration.

Because the sources on the surface are usually far from the target area, the resolution in the direction perpendicular to the wave propagation is limited. This can be quantitated by the radius of the Fresnel zone which can be calculated by:

$$r = \sqrt{\frac{Z\lambda}{2}}, \tag{3.2}$$

where, Z is the distance of an image point to the source, and λ is the dominate wavelength at the image point. As an example, for a point with 3000 m/s velocity and 5000 m away from the source, the resolution perpendicular to the wave propagation is about 274 m for VSP data with 100 HZ dominate frequency. This is much limited as compared to the resolution in the direction parallel to the wave propagation which is $\frac{\lambda}{2} = 7.5$ m.

Although the equation for VSP salt flank imaging by WEIM is equivalent to the equation for WEIM of VSP free-surface multiples, there are still some differences between them. One difficulty for VSP salt flank imaging is that the target reflections (reflections from the salt flank side, or rightgoing waves in Figure 3.1) can not be easily separated from the VSP data (remember, marine VSP free-surface multiples are often naturally well separated from strong VSP primaries if the water depth is deep enough, or they can be separated by a $f-k$ filtering). Using the unfiltered VSP data in IM will result in many artifacts. Despite these artifacts, the near borehole salt flank is usually the strongest vertical reflector, so imaging the salt flank is typically not a problem. The artifacts might not occur in the salt flank position, and they can usually be attenuated by stacking. In order to improve the migration image's S/N ratio, a wide distribution of sources on the surface can help, but its effect also depends on the structure of the overburden. Interestingly, usually the more complex is the overburden, the better is the imaging (Schuster et al., 2004).

3.3 Synthetic Experiment

A synthetic experiment is conducted to test WEIM for VSP salt flank imaging. Figure 3.2 shows a synthetic density model. There are 94 geophones evenly placed in the well from the depth 2700 m to 5500 m at a 30 m interval. Figure 3.3 shows a synthetic VSP common-shot gather with the source located on the surface and 5200 m to the right of

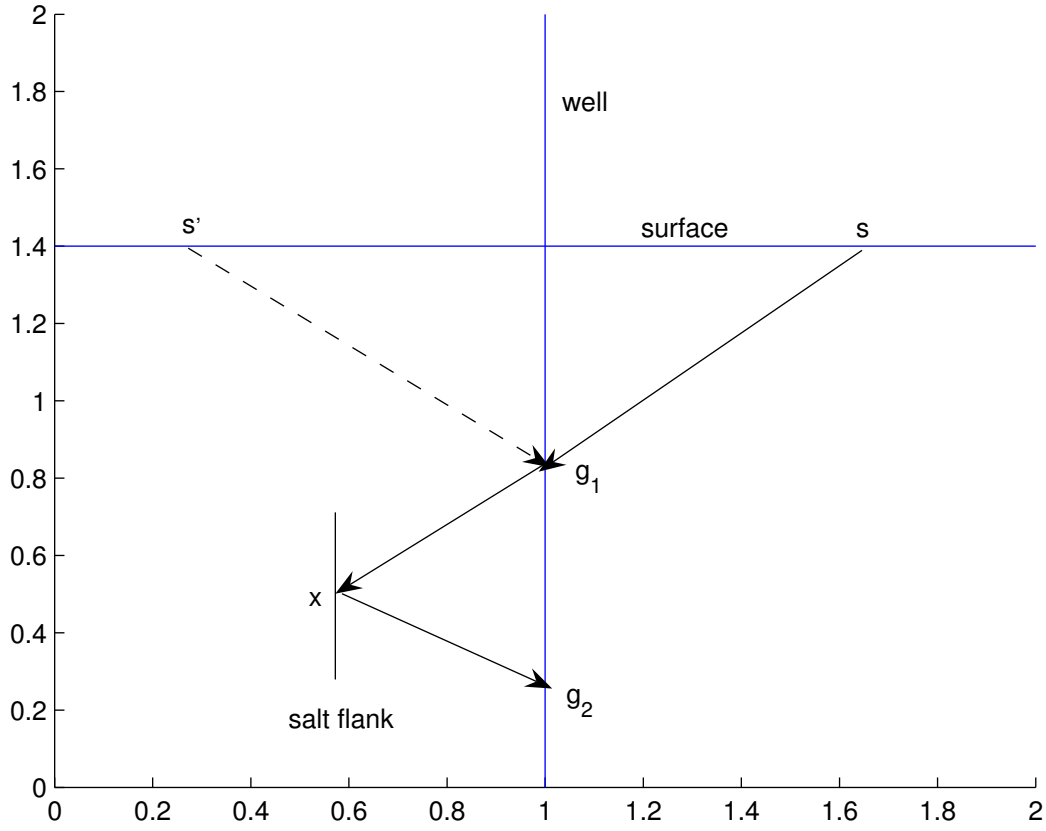

Figure 3.1. Ray diagram $\overline{\mathbf{sg}_1\mathbf{g}_2}$ for imaging a salt flank with VSP data. Rotating the figure counterclockwise by 90^o shows that the ray $\overline{\mathbf{s}'\mathbf{g}_1\mathbf{g}_2}$ is identical to the ray $\overline{\mathbf{sg}_1\mathbf{g}_2}$ in Figure 2.1 for VSP free-surface multiples. With interferometric methods, migrating the ray $\overline{\mathbf{s}'\mathbf{g}_1\mathbf{g}_2}$ is the same as migrating the ray $\overline{\mathbf{sg}_1\mathbf{g}_2}$ in this figure.

the well. These traces were computed by a finite-difference solution to the acoustic wave equation.

Figure 3.4 shows the actual velocity model of the target area. Without knowing the actual salt flank position, we use a local migration velocity model (Figure 3.5) that coincides with the target area. The left image of Figure 3.6 shows the WEIM result for one shot gather (shown in Figure 3.3), and the right image of Figure 3.6 shows the final WEIM result for ten shot gathers. From it we see, when the shot number increases, the S/N ratio is improved, but the image area remains the same.

From the above migration results, besides the salt flank image, there are also artifacts. Those artifacts are due to the phenomenon of cross talk because the unfiltered VSP data are used for migration. Here, cross talk (or virtual multiples) is defined as the accidental imaging of events that are not relevant, such as direct-primary correlations (Schuster et al., 2004). While it is challenging to separate the salt flank related reflections from the original VSP data, some numerical treatment for suppressing cross talk is possible (Muijs, et al, 2005).

3.4 Conclusion

The WEIM method is introduced for VSP salt flank imaging. Numerical results show that it is efficient and accurate in practice because a huge chunk of the overburden is bypassed during imaging. It is possible to image the salt flank by only one shot gather of VSP data, but more shot gathers are needed to improve the S/N ratio of the image. An implication of this work is that other major vertical structures, such as the San Andreas fault could also be imaged by interferometric methods. For field data applications, one caution is that out-of-plane 3D waves can distort the final image, and the inability to isolate target reflections from the VSP data can result in many artifacts. Therefore, 3D component geophones are recommended to isolate the out-of-plane reflections and target reflections.

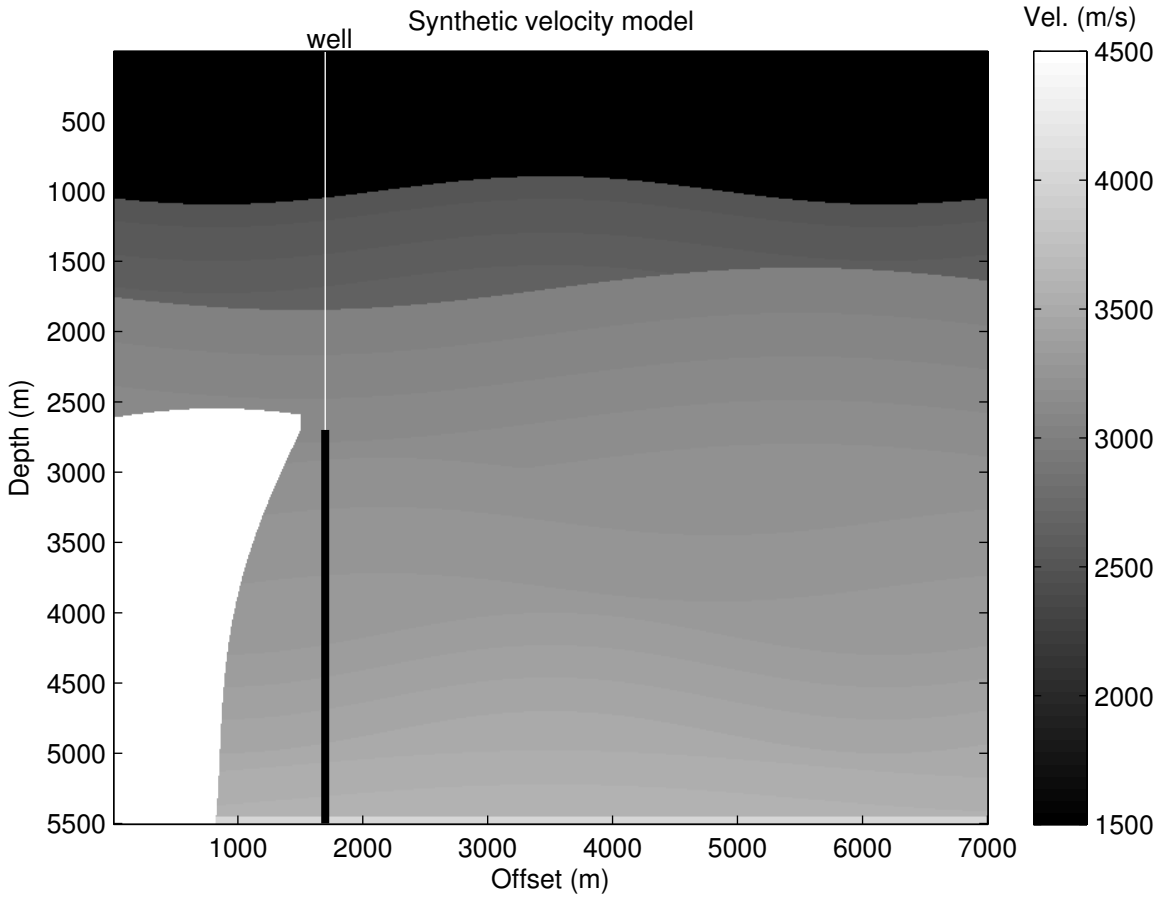

Figure 3.2. A synthetic velocity model for testing VSP salt flank imaging by WEIM. There are 94 geophones evenly placed in the well from the depth 2700 m to 5500 m at a 30 m interval. Sources are deployed on the surface.

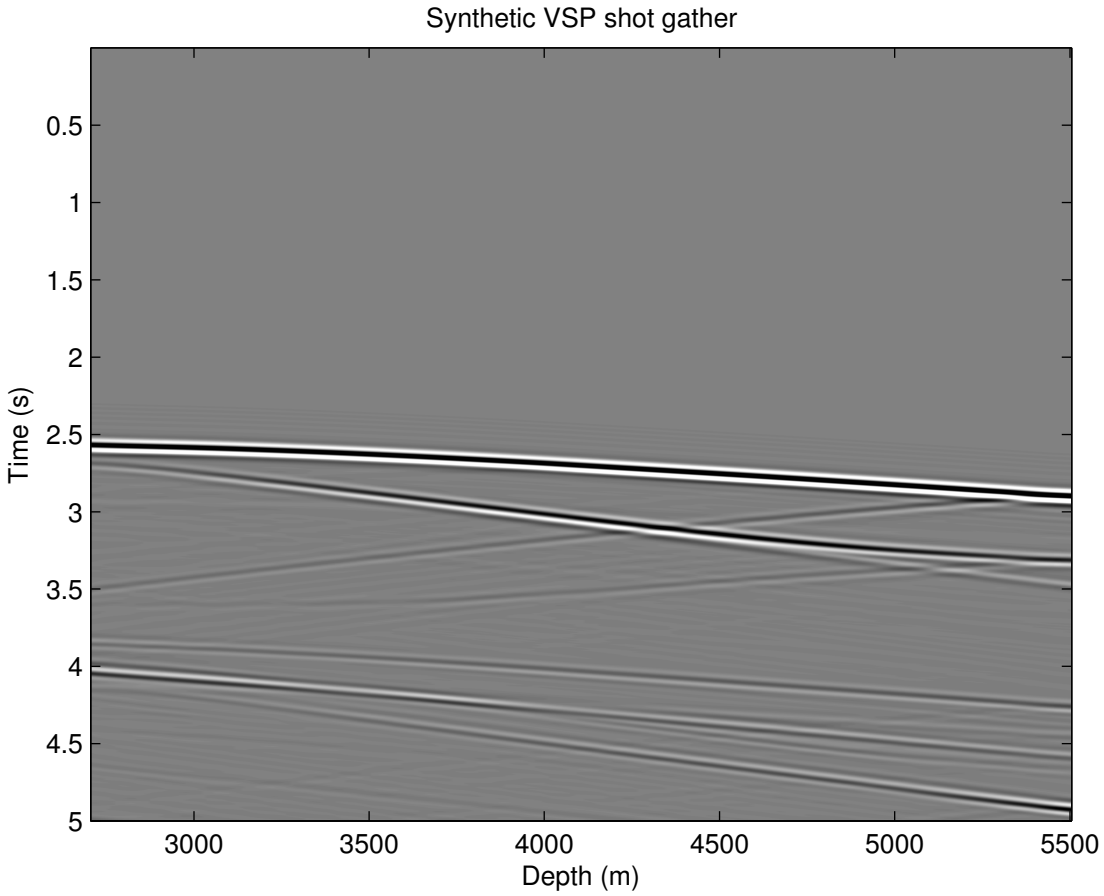

Figure 3.3. A finite-difference synthetic VSP common-shot gather (acoustic) for a source located on the surface with a lateral 4000 m offset from the well.

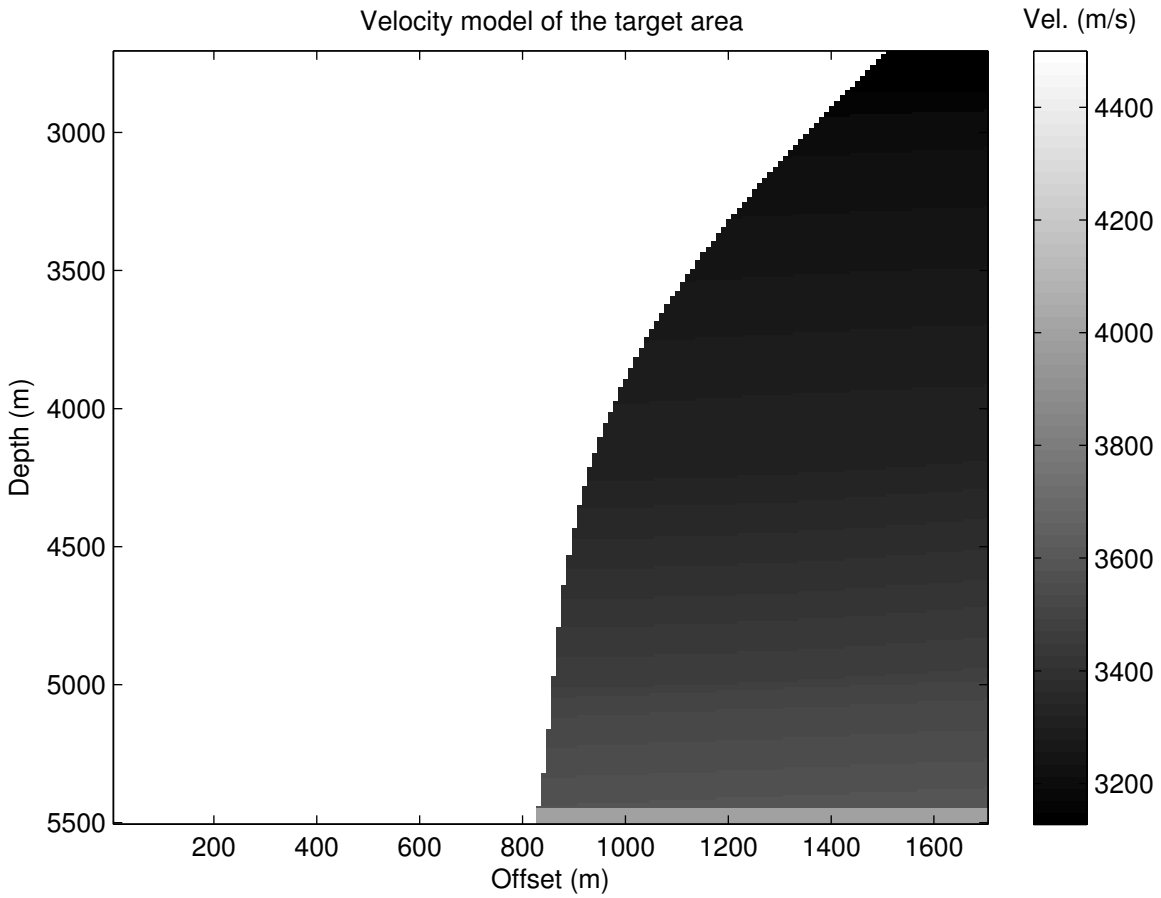

Figure 3.4. Salt flank velocity model.

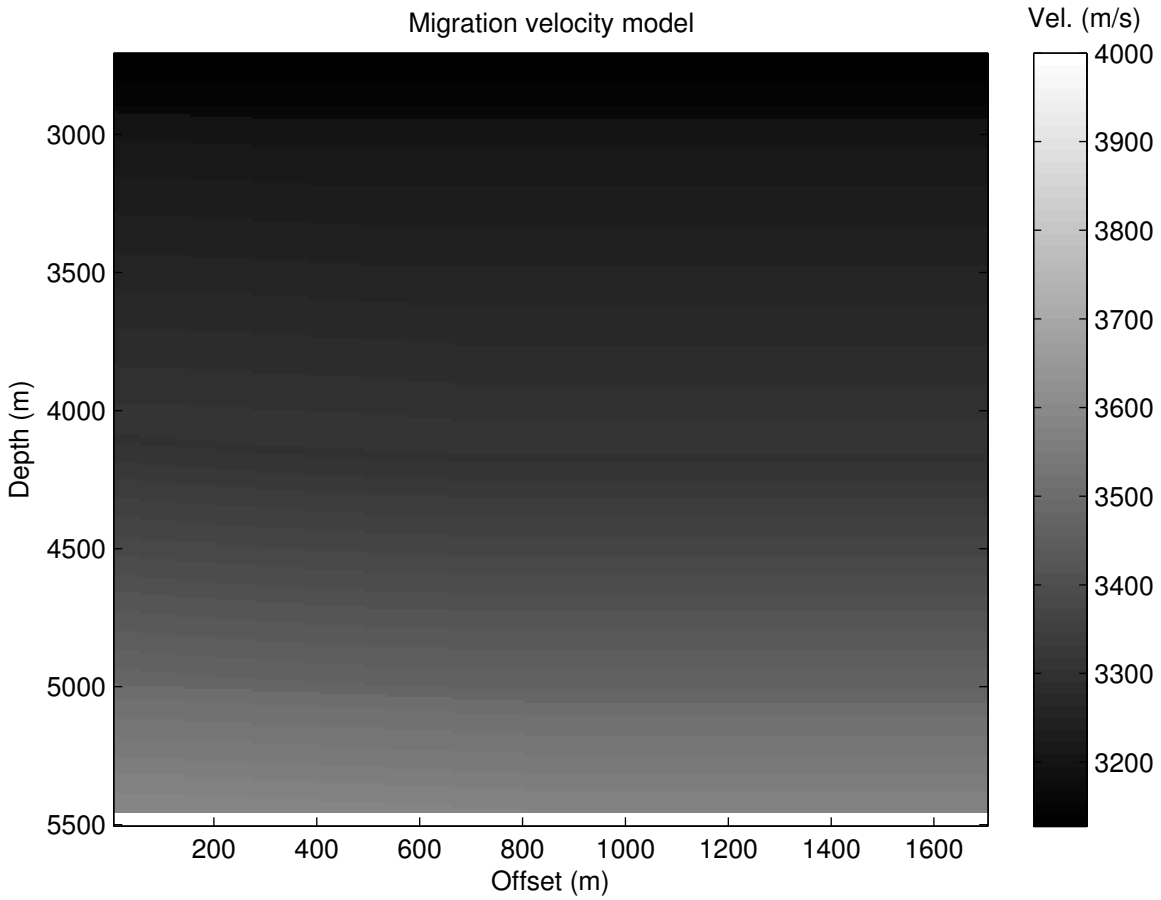

Figure 3.5. Local migration velocity model of the target area used for WEIM.

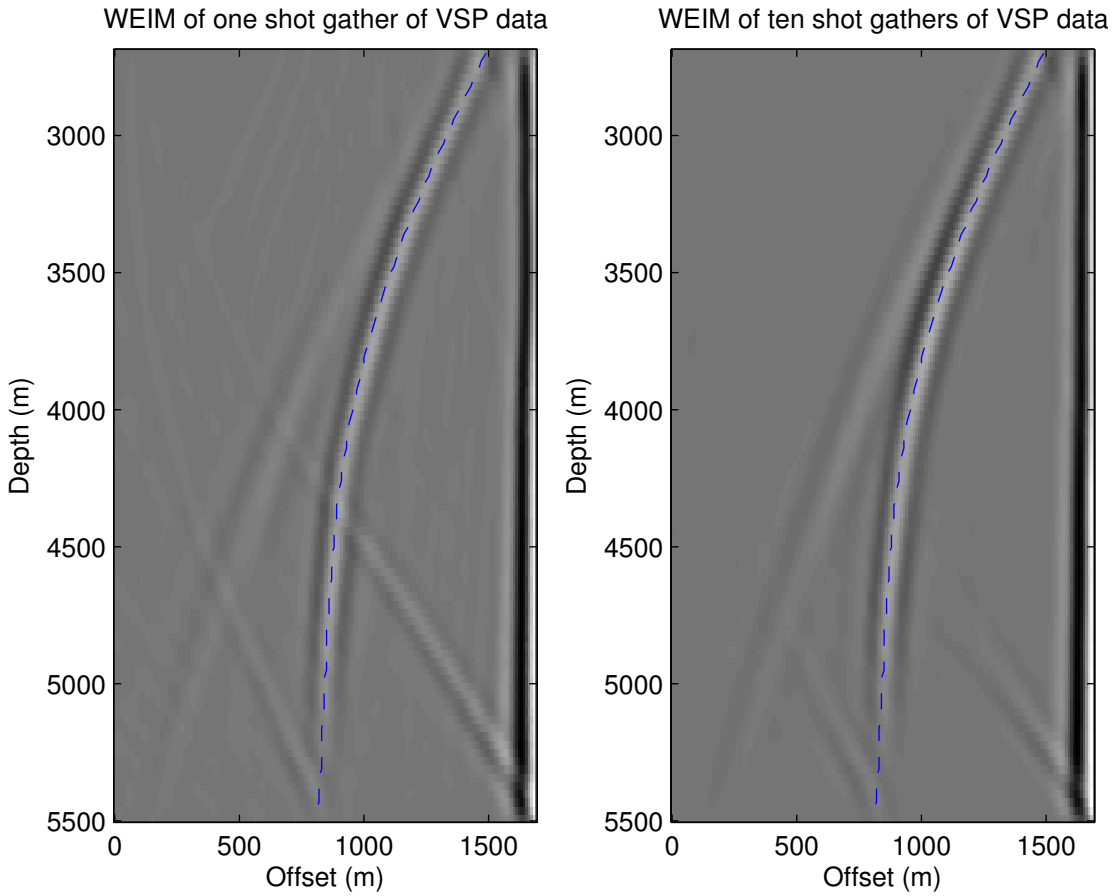

Figure 3.6. Results after WEIM of VSP data for (left) one shot gather, and (right) ten shot gathers. As expected, coherent artifacts are suppressed with an increase in number of shot gathers. The salt flank is delineated by dashed line.

REFERENCES

[1] Aki, K. and Richards, P. G., 2002, Quantitative seismology (2nd edition): University Science Books, Sausalito, California.

[2] Bakulin, A. and Calvert, R., 2004, Virtual source: new method for imaging and 4D below complex overburden: 74th Annual International Meeting, SEG, Expanded Abstracts, 2477-2480.

[3] Baysal, E., Kosloff, D. D., and Sherwood, J. W. C., 1983, Reverse-time migration: Geophysics, **48**, 1514-1524.

[4] Brandsberg-Dahl, S., Van Gestel, J-P., Etgen, J. T., and Hornby, B., 2003, VSP salt flank imaging through wavefield continuation: 65th Annual Conference, EAGE, Extended Abstracts, B14.

[5] Calvert, R., Bakulin, A., and Jones, T. C., 2004, Virtual source, a new way to remove overburden problems: 66th Annual Conference, EAGE, Extended Abstracts, P234.

[6] Claerbout, J., 1968, Synthesis of a layered medium from its acoustic transmission response: Geophysics, **33**, 264-269.

[7] Cole, S., 1995, Passive seismic and drill-bit experiment using 2-D arrays: Ph.D. thesis, Stanford University, Palo Alto, USA.

[8] Daneshvar, M. R., Clay, C. S., and Savage, M. K., 1995, Passive seismic imaging using microearthquakes: Geophysics, **60**, 1178-1186.

[9] Draganov, D., Wapenaar, K., Artman, B., and Biondi, B., 2004, Migration models for passive seismic data: 74th Annual International Meeting, SEG, Expanded Abstracts, 1123-1126.

[10] Duvall, T. L., Jefferies, S. M., Harvey, J. W., and Pomerantz, M. A., 1993, Time-distance helioseismology: Nature, **362**, 430–432.

[11] Gardner Gardner, L. W., 1949, Seismograph determination of salt-dome boundary using well detector deep on dome flank: Geophysics, **14**, 29-38.

[12] Gazdag, J., 1978, Wave equation migration with the phase-shift method: Geophysics, **43**, 1342-1351.

[13] Gazdag, J., and Sguazzero, P., 1984, Migration of seismic data by phase shift plus interpolation: Geophysics, **49**, 124-131.

[14] Giles, P. M., Duvall, T. L., and Scherrer, P. H., 1997, A subsurface flow of material from the sun's equator to its poles: Nature, **390**, 52.

[15] Gras, R., Tushingham, K., and Jamieson, G. A., 1998, Interpretation of the evolution of a salt body in the Gulf of Mexico: The Leading Edge, Vol. **17**, 1378-1385.

[16] Hale, D., Hill, N. R., and Stefani J., 1992, Imaging salt with turning seismic waves: Geophysics, **57**, 1453-1462.

[17] Hornby, B., 2006, VSP: beyond time-to-depth: The Leading Edge, Vol. **25**, 446-452.

[18] Hussein, S., Desler, J., and Miller G., 1997, Imaging salt substructures in the Gulf of Mexico using 3-D turning wave migration: The Leading Edge, Vol. **16**, 1487-1495.

[19] Jiang, Z., Yu, J., Schuster, G. T., and Hornby, B., 2005, Migration of multiples: The Leading Edge, Vol. **24**, No. 3, 315-317.

[20] Jiang, Z., 2006, Migration and attenuation of surface related and interbed multiples, Ph.D. thesis, University of Utah.

[21] Katz, L., 1990, Inverse vertical seismic profiling while drilling: United States Patent, Patent Number: 5,012,453.

[22] Li, Y., Faw, D., Jackson, J., and Dushman, D., 2002, Imaging of a salt face and truncating updip sands using offset VSP (OVSP) and a salt proximity survey (SPS) in the Gulf of Mexico: 72th Annual International Meeting, SEG, Expanded Abstracts, 2349-2352.

[23] McMechan, G.A., 1983, Migration by extrapolation of time-dependent boundary values: Geophys. Prosp., **31**, 413-420.

[24] McMechan, G.A., Hu, L., and Stauber, D., 1988, Determination of salt proximity by wave-field imaging of transmitted energy: Geophysics, **53**, 1109-1112.

[25] Muijs, R., Holliger, K., and Robertsson, J., 2005, Prestack depth migration of primary and surface-related multiple reflections: 75th Annual International Meeting, SEG, Expanded Abstracts, 2107-2110.

[26] O'Brien M. J., Gray, S. H., 1996, Can we image beneath salt? The Leading Edge, Vol. **15**, 17-22.

[27] O'Brien J., Amold R., Sixta D., Davies M. A., and Houghton P., 2005, Resolving the K-2 salt structure in the Gulf of Mexico: The Leading Edge, Vol. **24**, 404-409.

[28] O'Brien J., 2005 The sediment proximity survey, or how to find the salt flank: The Leading Edge, Vol. **24**, 415-420.

[29] Qin, F., Luo, Y., Olsen, K. B., Cai, W., Schuster, G. T., 1992, Finite-Difference solution of the eikonal equation along expanding wavefronts: Geophysics, **57**, 478-487.

[30] Rickett, J., and Claerbout, J., 1996: Passive seismic imaging applied to synthetic data: Stanford Exploration Project, **92**, 83-90.

[31] Rickett, J., and Claerbout, J., 1999: Acoustic daylight imaging via spectral factor-

ization: Helioseismology and reservoir monitoring: The Leading Edge, **18**, 957-960.

[32] Rickett, J., and Claerbout, J., 2000: Calculation of the acoustic impulse response by multi-dimensional spectral factorization: Solar Physics, **192**, no. 1/2, 203-210.

[33] Scherrer, P. H., Bogart, R. S., Bush, R. I., Hoeksema, J. T., Kosovichev, A. G., Schou, J., Rosenberg, W., Springer, L., Tarbell, T. D., Title, A., Wolfson, C. J., Zayer, I., and the MDI Engineering Team, 1995, The solar oscillations investigation - Michelson Doppler imager: Solar Physics, **162**, no. 1/2, 129–188.

[34] Schuster, G. T., 1999, Seismic interferometric imaging with waveforms: Utah Tomography and Modeling/Migration (UTAM) Consortium midyear report, 121-130.

[35] Schuster, G. T., and Rickett, J., 2000, Daylight imaging in V(x,y,z) media: Utah Tomography and Modeling/Migration (UTAM) Consortium midyear report, 49-70.

[36] Schuster, G. T., 2001, Theory of Daylight/Interferometric Imaging: Tutorial: 63rd Annual EAGE meeting, expanded Abstracts, A-32.

[37] Schuster, G. T., 2003, Migrating the most bounce out of multiples: 65th Annual Conference, EAGE, Extended Abstracts, P4.

[38] Schuster, G. T., Katz, L., Followill, F., and Yu, J., 2003, Autocorrelogram migration: Theory: Geophysics, **68**, 1685-1694.

[39] Schuster, G. T., Yu, J., Sheng, J., and Rickett, J., 2004, Interferometric/Daylight seismic imaging, Geophys. J. Int., **157**, 838-852.

[40] Snieder, R., Gret, A., Douma, H., and Scales, J., 2002, Coda wave interferometry for estimating nonlinear behavior in seismic velocity: Science, **295**, 2253-2255.

[41] Snieder, R., 2004, Extracting the Green's function from the correlation of coda waves: A derivation based on stationary phase: Phys. Rev. E, **69**, 046610.

[42] Stoffa, P. L., Fokkema, J. T., de Luna Freire R. M., and Kessinger, W. P., 1990, Split-step Fourier migration: Geophysics, **55**, 410-421.

[43] Wapenaar, K., Dragonov, D., and Fokkema, J., 2003, Synthesis of an inhomogeneous medium from its acoustic transmission response: Geophysics, **68**, 1756-1559.

[44] Whitmore, N. D., and Lines, L. R., 1986, Vertical seismic profiling depth migration of a salt dome flank, Geophysics, **51**, 1087-1109.

[45] Willis, M. E., Lu, R., Campman, X., Toksoz, M. N., Zhang, Y., and de Hoop, M. V., 2006, A novel application of time-reversed acoustics: Salt-dome flank imaging using walkaway VSP surveys: Geophysics Letters, **71**, A7-A11.

[46] Xiao, X., Zhou, M., Schuster, G. T., 2005, Salt flank delineation by PS interferometric imaging: 75th Annual International Meeting, SEG, Expanded Abstracts, 2029-2032.

[47] Yu, J., and Schuster, G. T., 2001, Crosscorrelogram migration of IVSPWD data: 71st Annual International Meeting, SEG, Expanded Abstracts, 456-459.

[48] Yu, J., Katz, L., Followill, F., and Schuster, G. T., 2003, Autocorrelogram migration: RVSP example: Geophysics, **68**, 297-307.

[49] Yu, J., and Schuster, G. T., 2006, Crosscorrelogram migration of inverse vertical seismic profile data: Geophysics, **71**, S1-S11.

[50] Zhang J. and McMechan G. A., 1994, 3-D transmission tomography using wide aperture data for velocity estimation for irregular salt bodies: Geophysics, **59**, 1620-1630.